Supplementary Online Material for

Elucidating CO_2 Dynamics in High-Entropy MOF-74 via Machine Learning Interatomic Potentials

Klichchupong Dabsamut[1,2]*, and Ching-Ming Wei[1]*

[1]Institute of Atomic and Molecular Sciences (IAMS), Academia Sinica, Taipei, 10617, Taiwan

[2]Department of Science, Technology and Innovation, Faculty of Science, Chulabhorn Royal Academy, Bangkok, Thailand

*E-mail: klichchupong.d@gmail.com, cmw@as.edu.tw

COMPUTATIONAL METHODS

Static DFT calculations

We used density functional theory (DFT) with the projector augmented wave (PAW) method in VASP, the Perdew-Burke-Ernzerhof (PBE) exchange correlation functional with Grimme-D3 dispersion, a plane wave cutoff of 500 eV, and spin polarized electrons. All energy and force convergence criteria were set to 1×10^{-5} eV and 0.02 eV $Å^{-1}$, respectively. A Monkhorst-Pack k-point mesh of 1×1×3 was used for Brillouin zone sampling in all systems. Geometry optimizations and single point SCF evaluations were performed with the same settings.

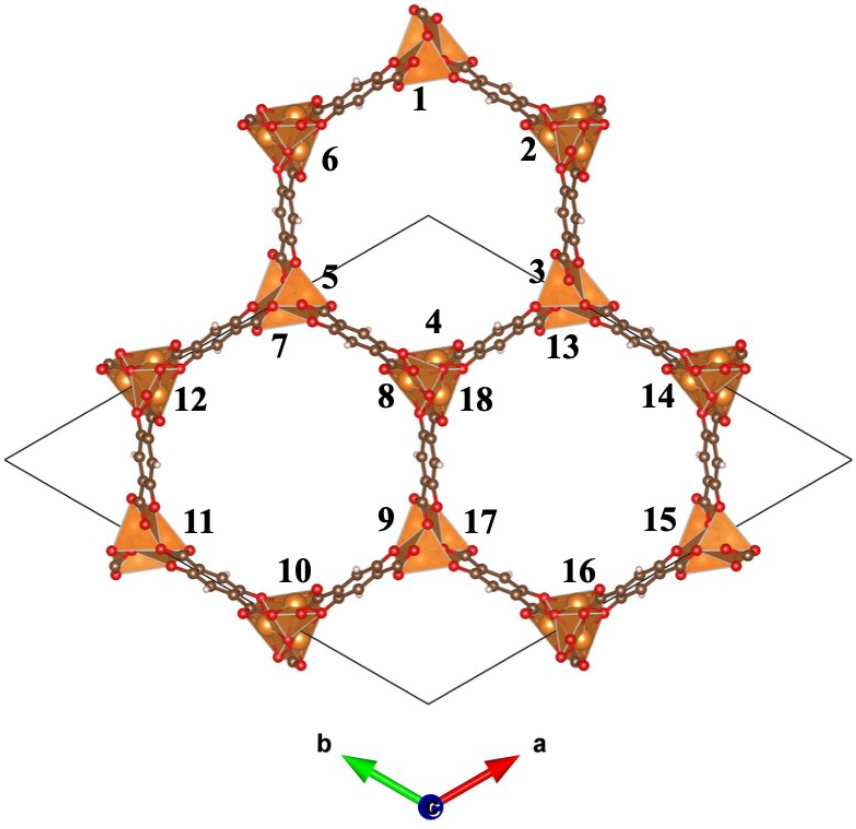

Figure S1. Crystal structure of MOF-74. The black outline marks one unit cell. Each unit cell contains three parallel channels along *c*, and each channel hosts six metal sites (18 metal sites in total).

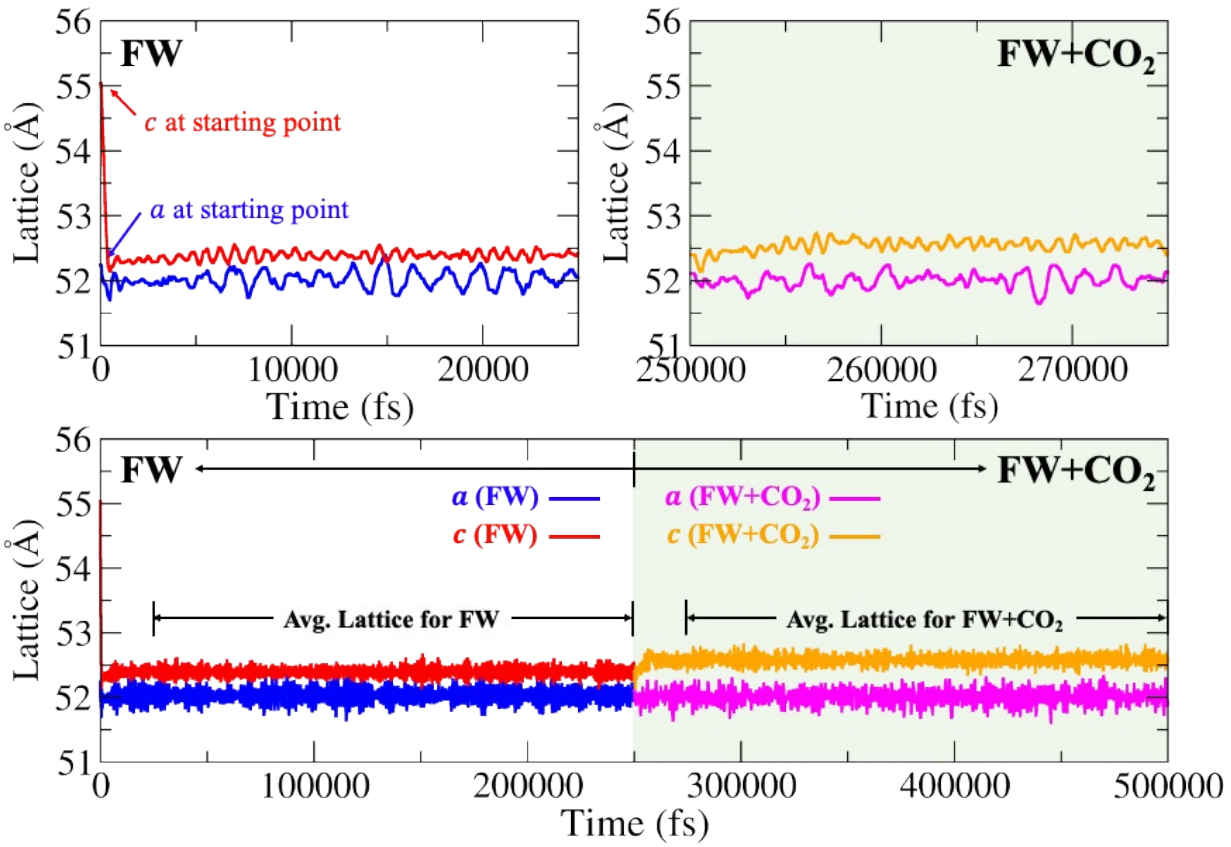

Figure S2. NPT equilibration of lattice parameters of 2×2×8 Mg-MOF-74 supercell at 300 K and 1 bar. The lower panels show the full trajectory: 0-250 ps for the empty framework (non-shaded area) and 250-500 ps after loading one CO_2 per metal site (shaded area). The upper panels zoom into 0-25 ps and 250-275 ps, illustrating the initial transients that were excluded from averaging.

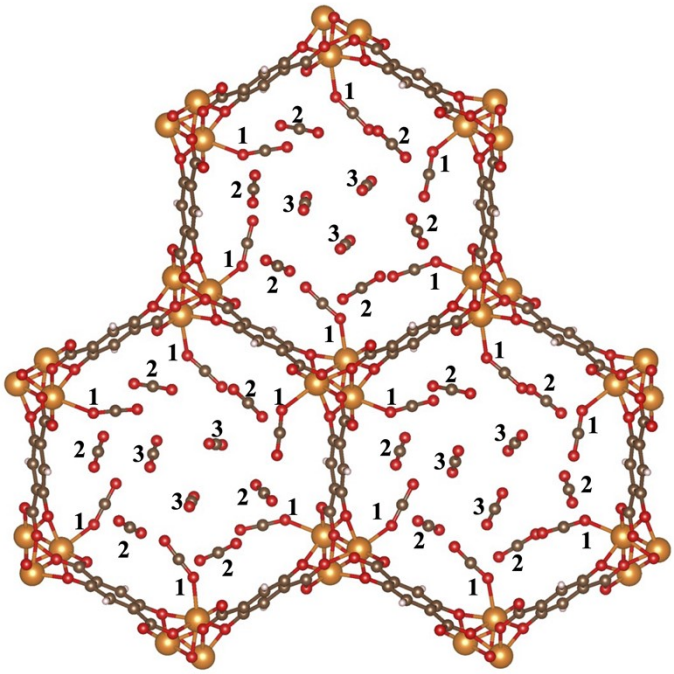

Figure S3. CO_2 adsorption regions in a MOF-74 unitcell at high loading. 1 = OMS (open metal site), 2 = IMS (inter metal site), and 3 = CCS (channel-center site).

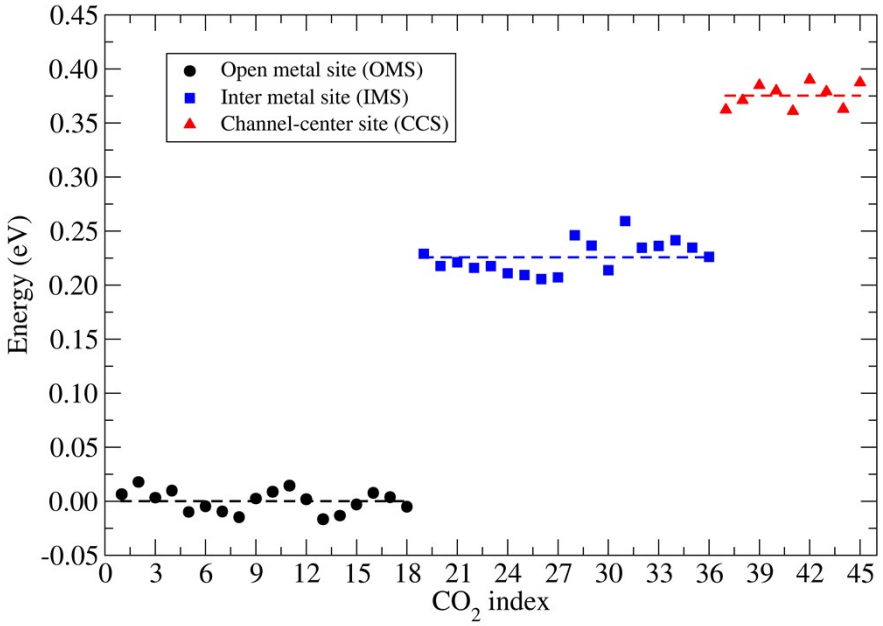

Figure S4. Site resolved single point energies for CO_2 in Mg-MOF-74, extracted from the 45 CO_2 optimized structure, energies referenced to the OMS mean, dashed lines indicate the mean for each site type.

Table S1. Average formation energies for the 20 unique permutations of the Mg–Co–Cu–Ni–Zn ratio in the MOF-74 unitcell. Each value is the average of five random metal-site assignments per permutation. Formation energies are referenced to isolated-atom energies for Mg, Co, Cu, Ni, and Zn, to graphene for C, to O_2 molecule for O and to H_2 molecule for H. all computed with the same DFT settings.

Mg–Co–Cu–Ni–Zn	DFT formation energy (eV)
5–4–3–3–3	-0.860
5–3–4–3–3	-0.859
5–3–3–4–3	-0.858
5–3–3–3–4	-0.868
4–5–3–3–3	-0.834
3–5–4–3–3	-0.806
3–5–3–4–3	-0.806
3–5–3–3–4	-0.815
4–3–5–3–3	-0.831
3–4–5–3–3	-0.805
3–3–5–4–3	-0.803
3–3–5–3–4	-0.814
4–3–3–5–3	-0.831
3–4–3–5–3	-0.804
3–3–4–5–3	-0.803
4–3–3–3–5	-0.849
3–4–3–3–5	-0.823
3–3–4–3–5	-0.822
3–3–3–5–4	-0.812
3–3–3–4–5	-0.822

Table S2. Summary of the training data and validation data by MLIP model. The active-learning method and selection criteria are given in the main text.

MLIP	Training set	
	Candidates	Selected for training
Model 1	2637	2637
Model 2	2990	2062
Model 3	3029	1312
Model 4	8409	1563
Total	17065	7574
MLIP	Validation set	
Model 1 - 4	1799	

Table S3. Equilibrium lattice constants (Å) for single-metal MOF-74 at 300 K and 1 bar from NPT simulations (MLIP), compared with DFT and experiment.

Lattice	Mg-MOF-74	Co-MOF-74	Cu-MOF-74	Ni-MOF-74	Zn-MOF-74
a (MLIP)	26.020	25.928	26.171	25.607	26.054
a (DFT)	26.119	26.172	26.250	25.632	26.206
a (EXPT.)	25.85-26.05	25.80-25.95	25.997	25.70-25.80	25.85-25.94
c (MLIP)	6.900	6.639	6.444	6.460	6.705
c (DFT)	6.879	6.757	6.284	6.752	6.796
c (EXPT.)	6.72-6.87	6.80-6.83	6.259[3]	6.73-6.80	6.80-6.84

References for experimental values:

[1]Kim, Ki-Joong, *et al. ACS Applied Materials & Interfaces* 13.29 (2021): 35223-35231.

[2]Dietzel, Pascal DC, *et al. Angewandte Chemie* 117.39 (2005): 6512-6516.

[3]Sanz, Raúl, *et al. Dalton Transactions* 42.7 (2013): 2392-2398.

[4]Vornholt, Simon M.*, et al. Chemistry–A European Journal* 27.33 (2021): 8537-8546.

[5]Molina, M. Asuncion, *et al. Microporous and Mesoporous Materials* 319 (2021): 110973.

[6]Yu, Decai, et al. *Chemical Science* 4.9 (2013): 3544-3556.

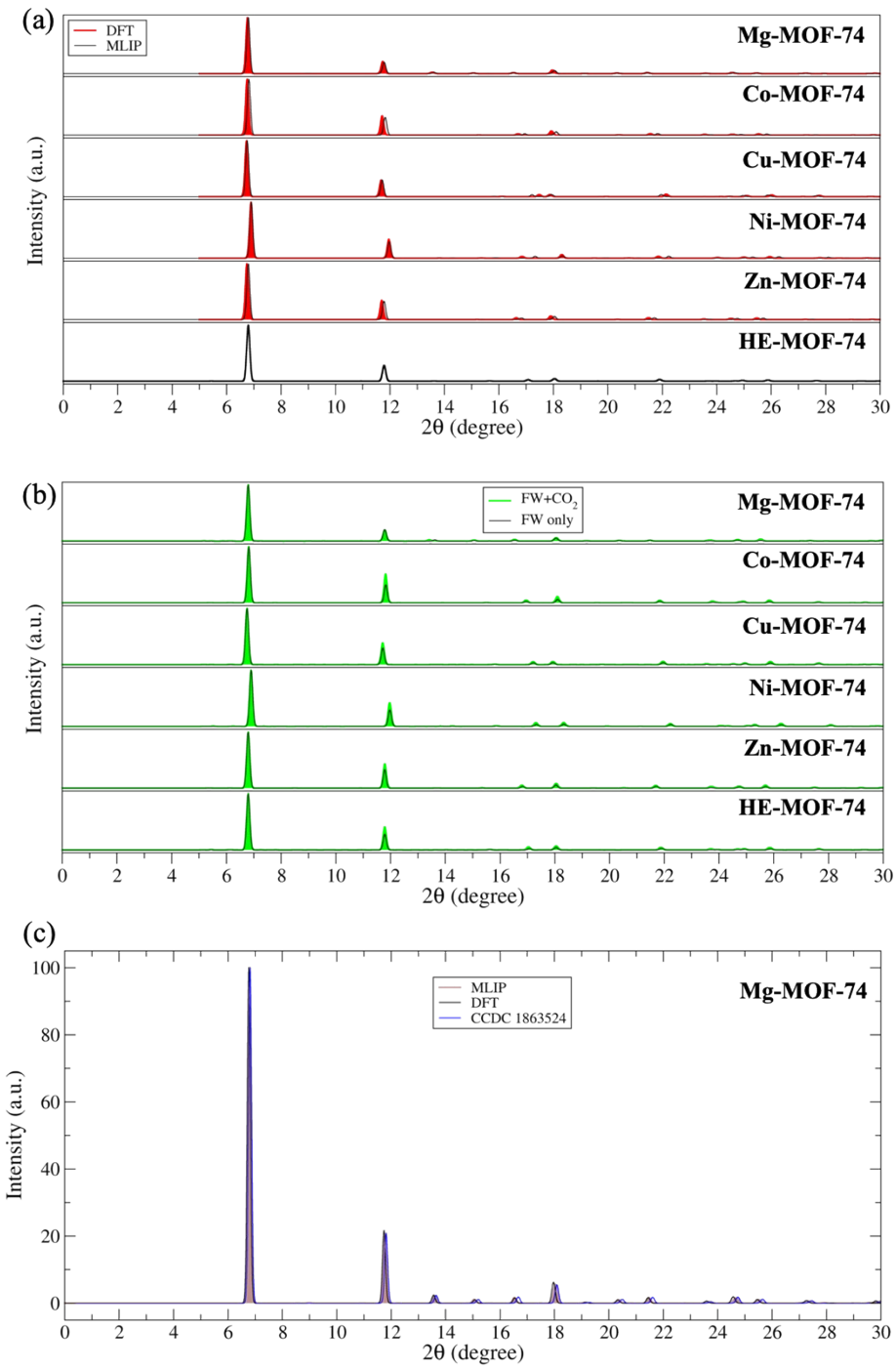

Figure S5. Simulated powder X-ray diffraction patterns of MOF-74 systems. (a) Comparison of DFT-optimized structures and MLIP-relaxed structures. (b) Framework-only versus CO_2-loaded structures. (c) Comparison of simulated patterns from MLIP-relaxed and DFT-optimized Mg-MOF-74 with the experimental reference structure (CCDC 1863524).

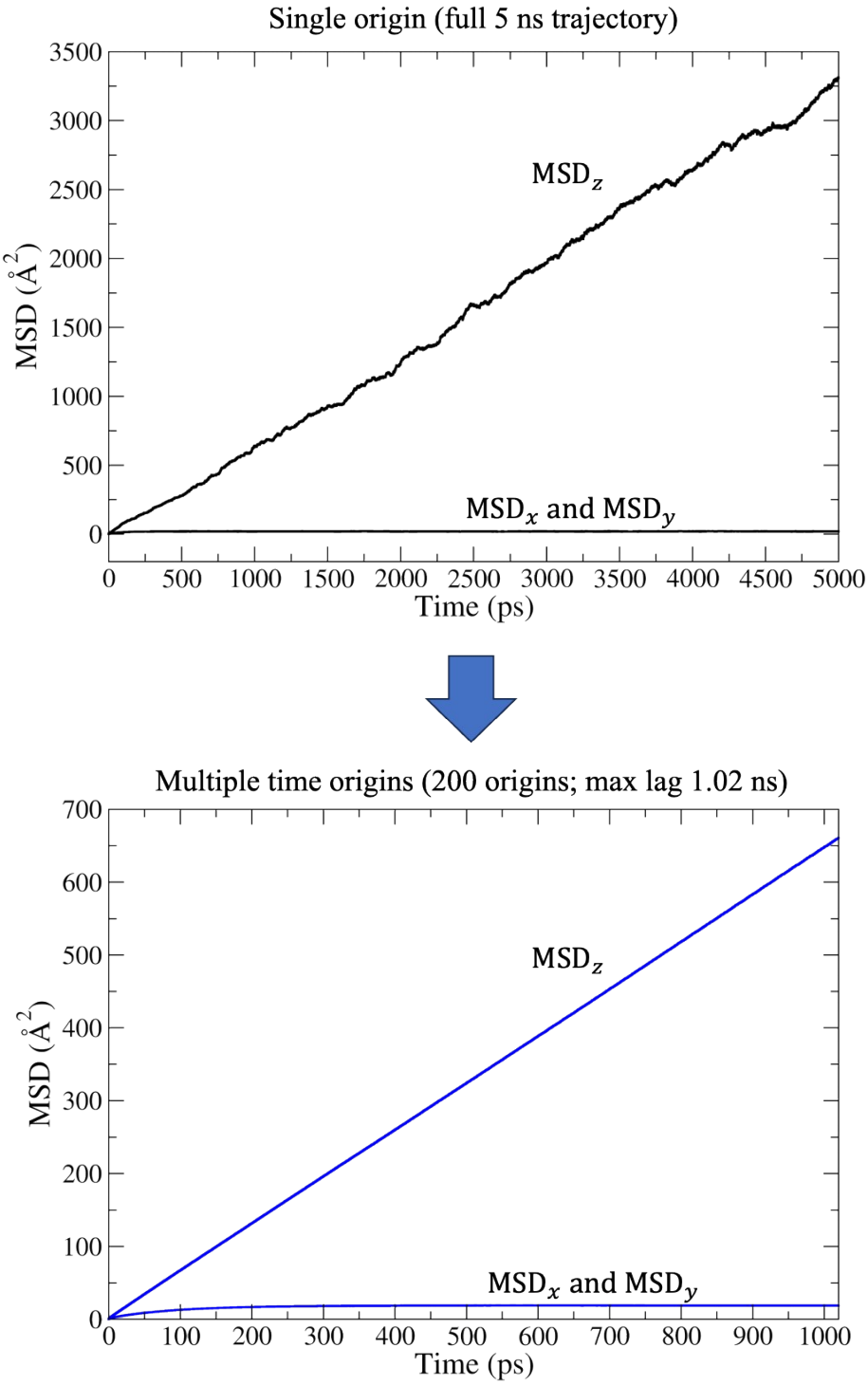

Figure S6. Effect of multiple time origins on MSD calculations. Upper: single-origin MSD computed over the full 5 ns trajectory, which shows increasing noise at long lag times. Lower: MSD averaged over 200-time origins spaced by 20 ps, with a maximum lag time of 1.02 ns, yielding a clean linear regime for diffusion analysis.

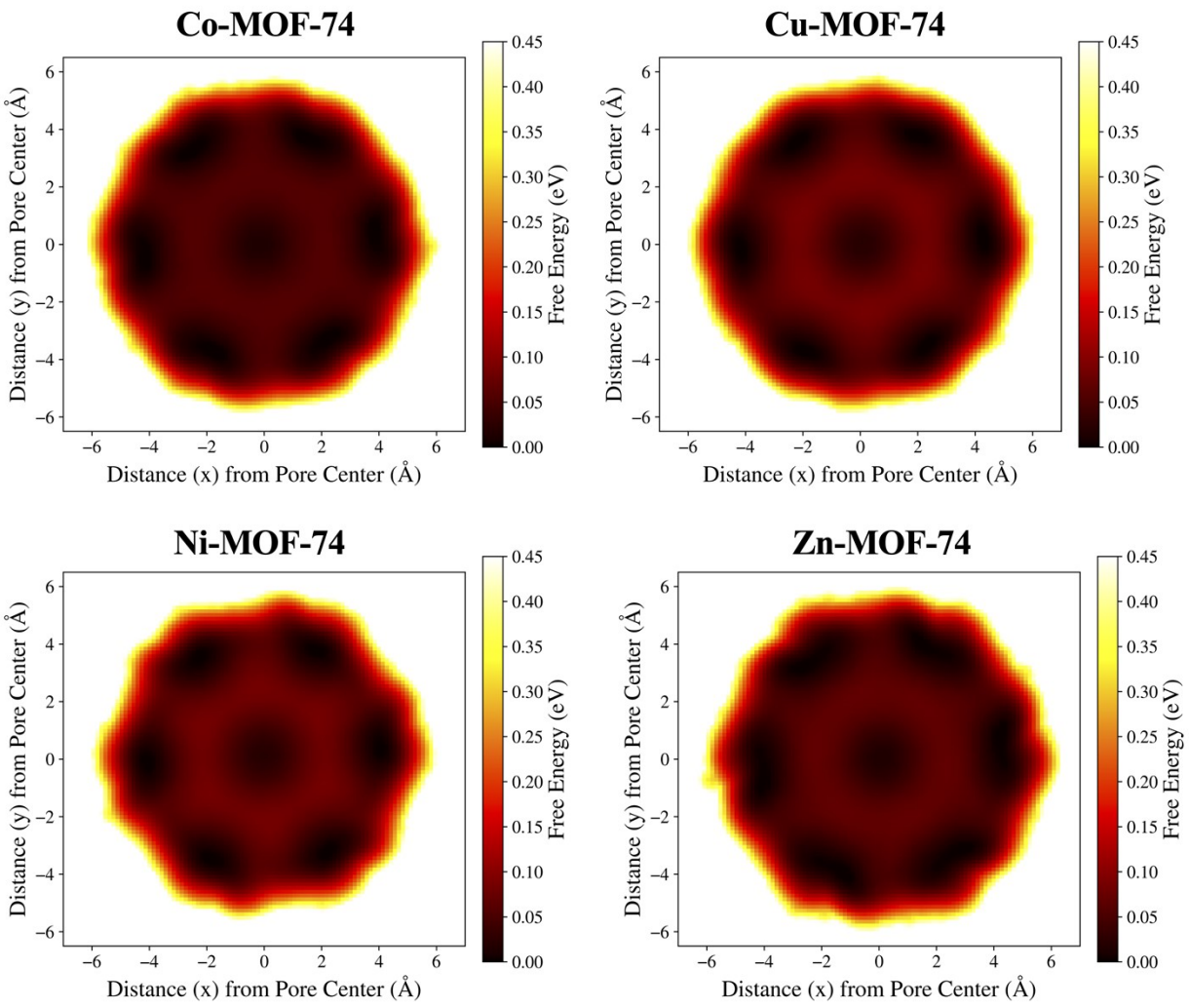

Figure S7. Free-energy landscapes of CO_2 in Co-, Cu-, Ni-, and Zn-MOF-74 at 300 K. The global minimum energy in each map is set to 0 eV as the reference.

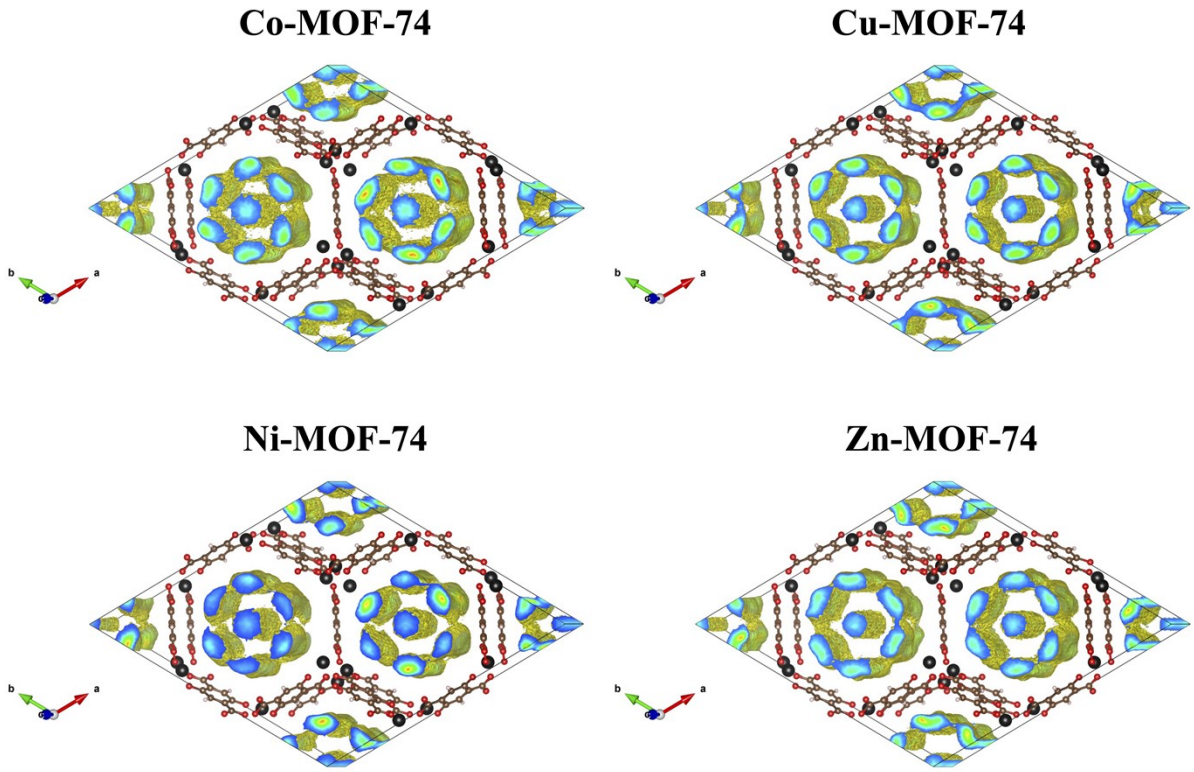

Figure S8. Atomic-density distribution functions (ADDFs) of CO_2 carbon positions of Co-, Cu-, Ni- and Zn-MOF-74, mapped from the 2×2×8 simulation supercell back to a single unit cell and displayed as a 1×1×2 supercell. Isosurfaces are set with the same value for all systems.

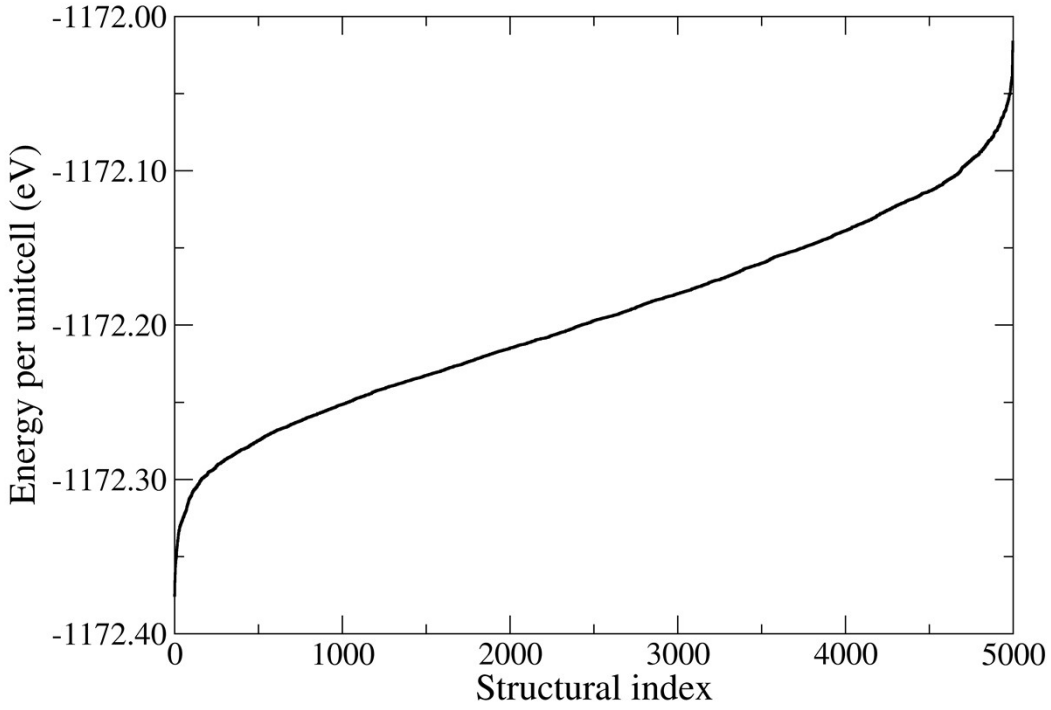

Figure S9. MLIP-predicted energy per unit cell for 5000 unique HE-MOF-74 configurations generated by random assignment of Mg, Co, Cu, Ni, and Zn on the metal sublattice.

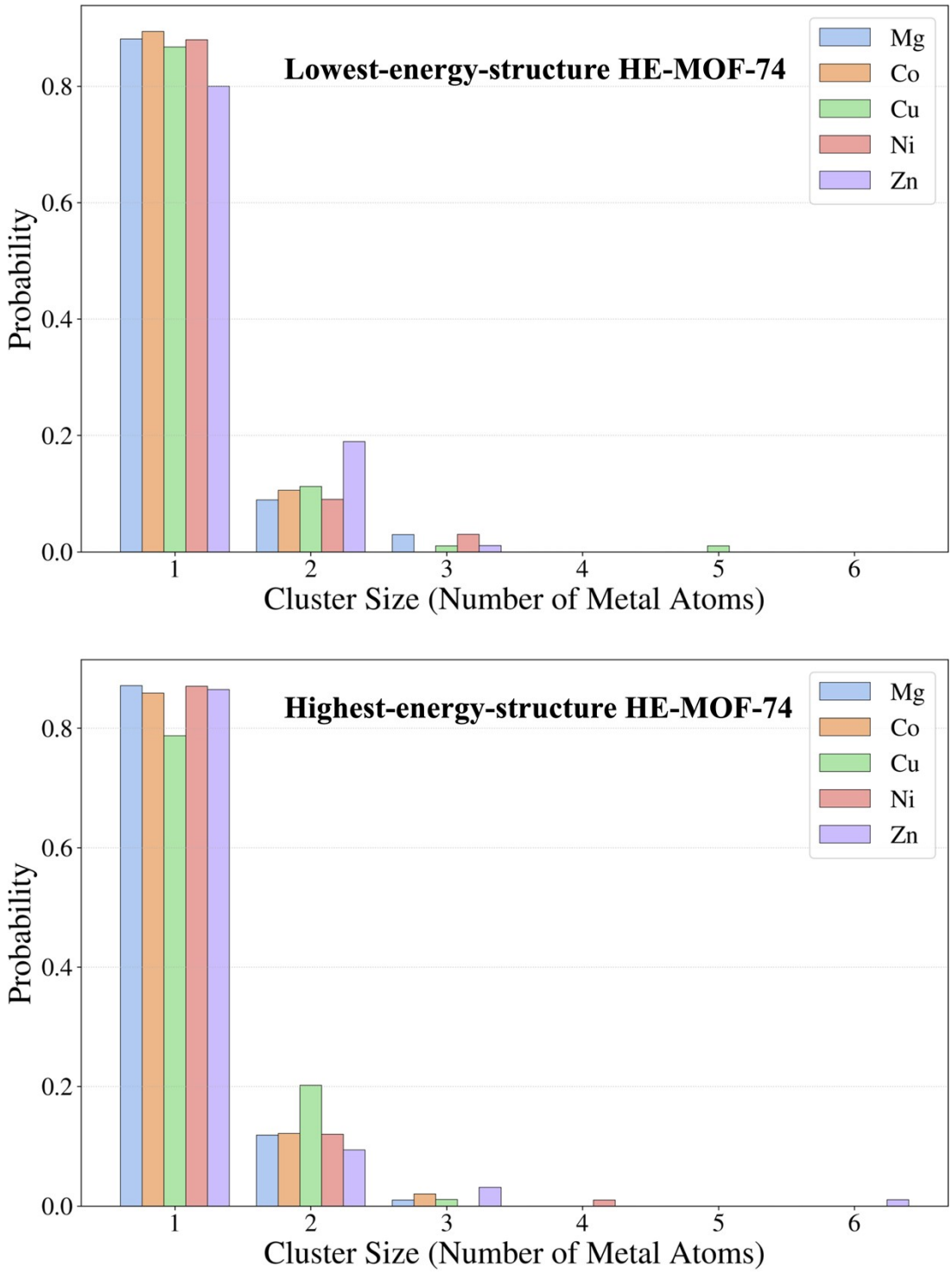

Figure S10. Metal-cluster analysis for HE-MOF-74 in the lowest-energy (top) and highest-energy (bottom) configurations selected from the 5000 random decorations. Clusters are defined using a 3.5 Å metal–metal cutoff.

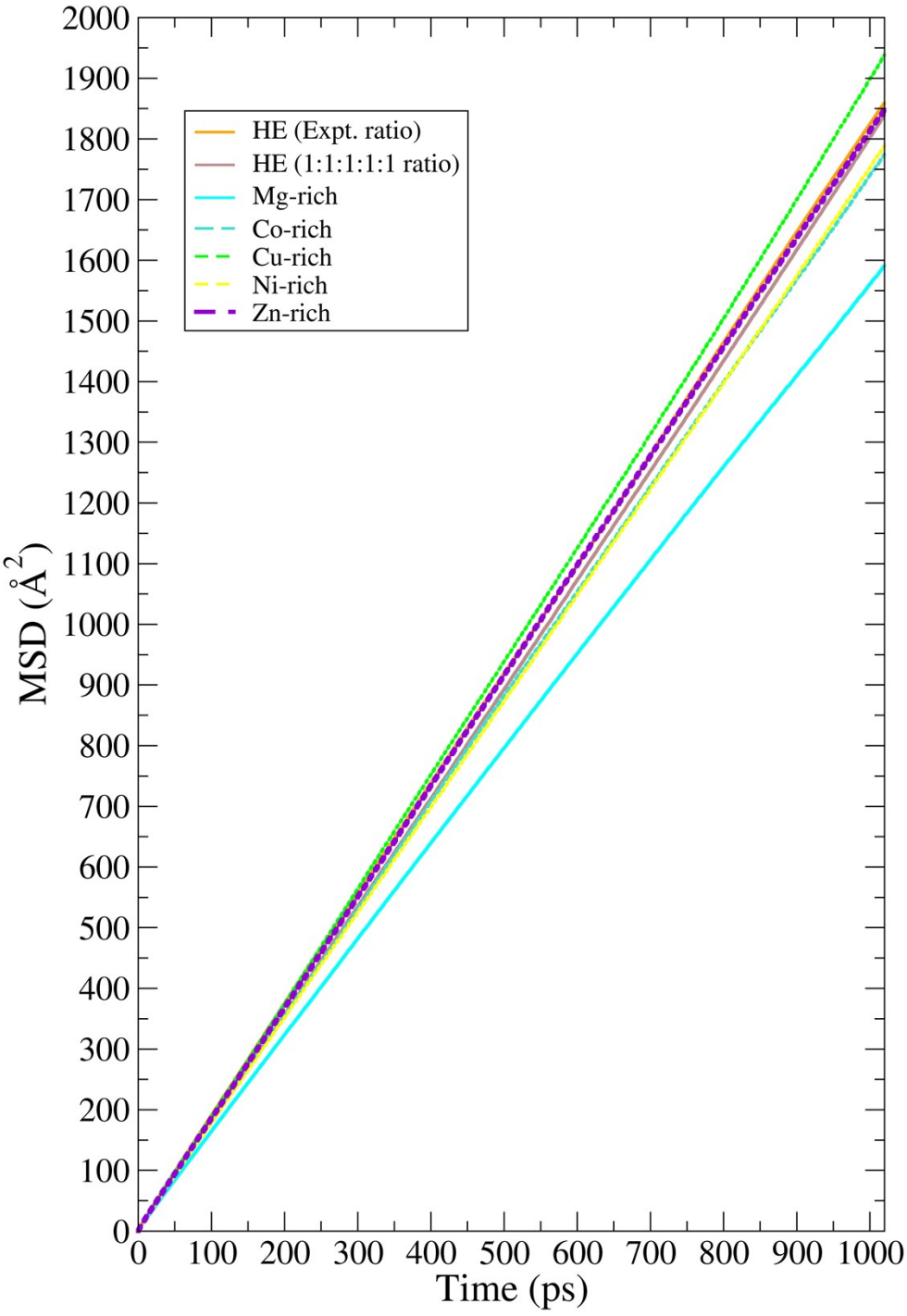

Figure S11. Mean-squared displacement (MSD) along the channel direction (z) for CO_2 in high entropy MOF-74 with different metal ratio at 300 K under saturation-level loading. Calculations use multiple time-origin averaging on a 5 ns NVT trajectory, resulting in a maximum lag of 1.02 ns.

Table S4. Equivalent gravimetric uptake at full primary-site loading (18 CO_2 per unit cell), reported as mmol CO_2 per g of framework.

System	mmol/g
Mg-MOF-74	8.240
Co-MOF-74	6.411
Cu-MOF-74	6.421
Ni-MOF-74	6.227
Zn-MOF-74	6.157
HE-MOF-74	6.615

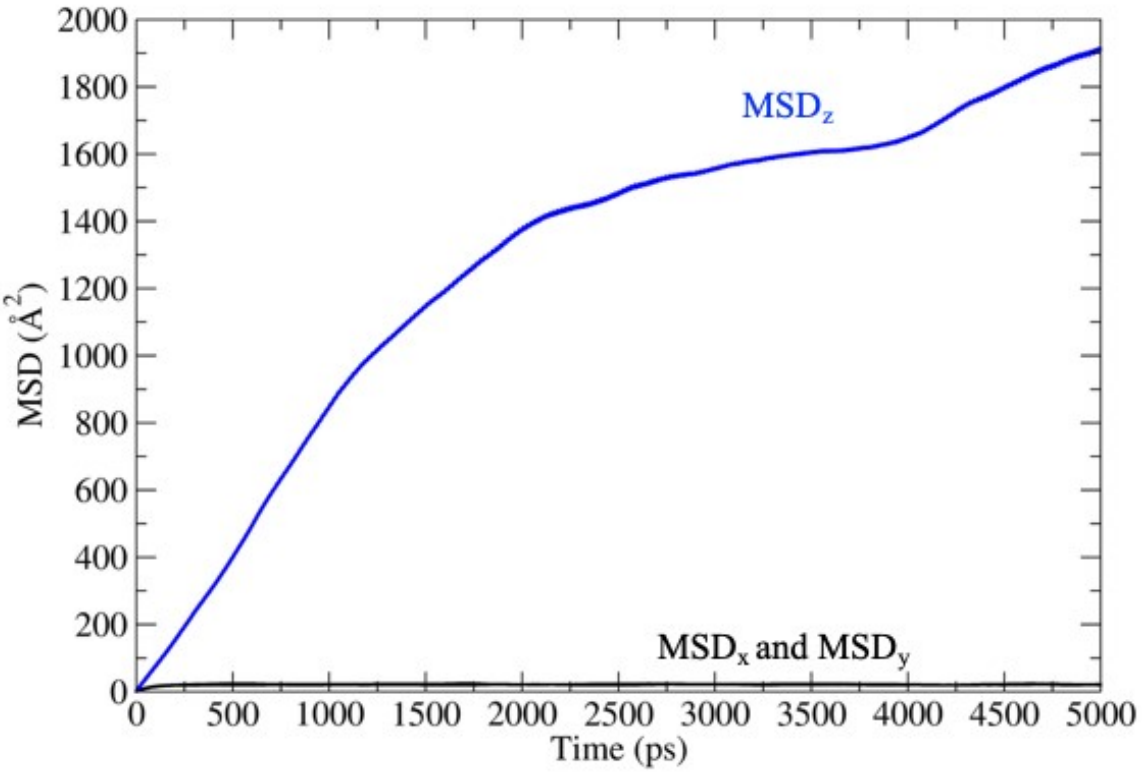

Figure S12. Mean-squared displacement (MSD) along the channel direction (z) for a single CO_2 molecule in Mg-MOF-74 at 300 K in the dilute limit (one CO_2 in a 1×1×2 cell). The trajectory length is 25 ns (NVT). MSD was evaluated using multiple time-origin averaging and is shown over a 5 ns lag window; the diffusion coefficient D_z was obtained by fitting the linear regime after excluding the first 1 ns of the averaged MSD curve.

Table S5. Supplementary axial diffusion coefficients, D_z in $\times 10^{-8}$ m^2/s, for single-metal MOF-74, HE-MOF-74, and the corresponding rule-of-mixtures (R.O.M.) estimate at 3, 18, and 24 CO_2 per unit cell. The 3 and 24 CO_2 per unit cell results were obtained from supplementary MLIP-based MD simulations in a 1×1×2 supercell at 300 K using 10 ns trajectories, whereas the 18 CO_2 per unit cell values are the main-text results from 2×2×8 supercell simulations.

MOF-74	3 CO_2/unitcell	18 CO_2/unitcell	24 CO_2/unitcell
Mg	0.106	0.322	0.316
Co	5.998	1.099	0.936
Cu	3.779	1.211	1.132
Ni	3.339	0.788	0.582
Zn	2.476	0.934	0.772
HE	2.900	0.899	0.705
HE (R.O.M.)	3.055	0.871	0.736

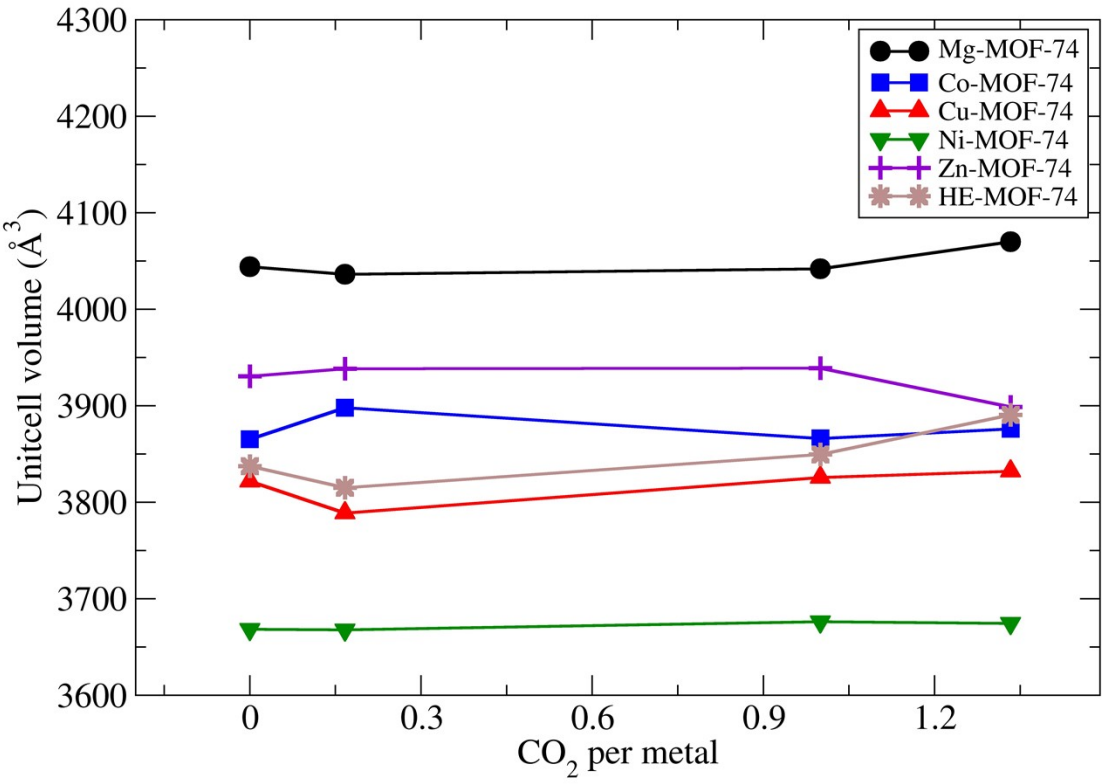

Figure S13. Unit-cell volumes of single-metal and HE-MOF-74 predicted at different CO_2 loadings per metal site.

Table S6. Comparison of experimental $-Q_{st}$, literature theoretical $-\Delta H$, and the present E_{ads}values from DFT and MLIP for CO_2 adsorption in single-metal MOF-74. The present DFT and MLIP adsorption energies were calculated for one CO_2 adsorbed in one MOF-74 unit cell.

	Exp. $-Q_{st}$ (eV)[1]	Theory $-\Delta H$ (eV)[1]	E_{ads} from DFT (eV)	E_{ads} from MLIP (eV)
Mg-MOF-74	-0.451	-0.424	-0.406	-0.295
Co-MOF-74	-0.348	-0.350	-0.241	-0.164
Cu-MOF-74	-0.229	-0.281	-0.171	-0.159
Ni-MOF-74	-0.400	-0.387	-0.222	-0.182
Zn-MOF-74	-0.278	-0.313	-0.290	-0.225

[1]Queen, Wendy L., et al. *Chemical Science* 5.12 (2014): 4569-4581